TNO report
FEL-96-B265

Conjugate gradient schemes for motion estimation in image sequences

TNO Physics and Electronics Laboratory

Oude Waalsdorperweg 63
PO Box 96864
2509 JG The Hague
The Netherlands

Phone +31 70 374 00 00
Fax +31 70 328 09 61

Date
February 1997

Author(s)
A.P. Berkhoff

Classification

Classified by	:	J.P. van Bezouwen
Classification date	:	29 January 1997

Title	:	Ongerubriceerd
Managementuittreksel	:	Ongerubriceerd
Abstract	:	Ongerubriceerd
Report text	:	Ongerubriceerd

Copy no	:	8
No of copies	:	23
No of pages	:	27 (excl RDP & distribution list)
No of appendices	:	-

All information which is classified according to Dutch regulations shall be treated by the recipient in the same way as classified information of corresponding value in his own country. No part of this information will be disclosed to any party.

The classification designation Ongerubriceerd is equivalent to Unclassified, Stg. Confidentieel is equivalent to Confidential and Stg. Geheim is equivalent to Secret.

The TNO Physics and Electronics Laboratory is part of TNO Defence Research which further consists of:

TNO Prins Maurits Laboratory
TNO Human Factors Research Institute

Netherlands Organization for Applied Scientific Research (TNO)

Managementuittreksel

titel	: Conjugate gradient schemes for motion estimation in image sequences
auteur(s)	: A.P. Berkhoff
datum	: februari 1997
Opdrachtnr.	: -
IWP-nr.	: 771
Rapportnr.	: FEL-96-B265

Dit rapport beschrijft methoden voor de schatting van locale beweging in een reeks opeenvolgende beelden. De methoden zijn gebaseerd op een globale minimalisatie van een relevant foutcriterium m.b.v. de conjugate gradient techniek. De expansie van het verplaatsingsveld geschiedt door het gebruik van basisfuncties volgens een Fourier-transformatie of een cosinus/sinus-transformatie in plaats en tijd. Deze representaties leveren automatisch een continu verplaatsingsveld op waarbij subpixel verplaatsingen gedetecteerd kunnen worden. Het foutcriterium kan worden gebaseerd op een verplaatsingsvector voor ieder beeldelement, maar ook op daarvan afgeleide gelineariseerde versies in vectoriële en scalaire vorm, afhankelijk van het gewenste compromis tussen rekentijd en nauwkeurigheid.

Contents

1 Introduction

1.1 Motion estimation methods

In the past, a large number of methods has been developed for the estimation of motion in image sequences. An early method is to search for the maximum of the cross-correlation function [1, 2]. This method might be less suitable if the images contain a relatively large amount of low-frequencies [3]. Other methods were based on a local minimization of the displaced frame difference [4, 5]. Block-wise minimization of a uniform error criterion was also suggested [3]. The latter block-matching methods have the advantage that they are very suitable for implementation on a single integrated circuit. Therefore, block-matching methods are often preferred for video compression schemes [6, 7]. Most implementations and standards use only one resolution level, but multiresolution block-matching schemes are being used more frequently now [8].

Some authors have suggested the use of edge feature detectors [9], as well as other feature detection methods [10]. For low-resolution and/or noisy images, these methods might be less suitable. Linearized forms of the displaced frame difference methods are the gradient methods [11]. A difficulty associated with the gradient methods is the aperture problem, i.e. ill-posed problem of finding the velocity vectors normal to the object boundaries. To overcome the latter problems, additional smoothness constraints have been used [12, 13]. The aperture problem is not limited to gradient methods. It also manifests itself in, for instance, block-matching schemes.

Several methods try to imitate the human visual system to a certain extent. Methods using activation profiles were discussed by Waxman [14]. Spatiotemporal filters using Gaussian bandpass filters were shown to be quite robust [15], at the cost of high computational requirements. The local phase in these filters can be used to arrive at stable motion estimation schemes [16–18]. Combinations of correlation methods with relaxation-labeling methods were suggested in [19]. The trend is that more and more motion estimation schemes are first trying to detect the contours or objects and then try to perform motion estimation [20]. However, more work needs to be done to arrive at stable and efficient methods.

1.2 Desired properties

Desirable properties of methods which are intended to determine motion between images are described by [21]. The methods which are pertinent to our problems are:

- Multiresolution property. The motion estimation methods should be able to estimate velocity vectors over a large magnitude range. In addition, the methods should be able to handle a large range of object sizes.
- Modest memory requirements. Global optimization methods often lead to the solution of a large number of linear equations. The solution to this system of equations is only possible for a small number of unknowns if direct matrix inversion methods are used due to the prohibitive storage requirements.
- Computational efficiency. The real-time constraint for contemporary video formats imposes considerable difficulties, even for relatively simple methods.
- Subpixel accuracy. Most hardware implementations only calculate integer displacements, which might not be sufficient.
- Convergence. Because of the large number of unknowns, many motion estimation schemes are based on iterative schemes. The convergence of these schemes is not always garanteed, however. This might lead to strange motion vector estimates.
- Robustness. The main application area of our motion estimation algorithms is motion detection. The primary objective is to create a robust system, rather than to provide a system which yields, for example, very accurate motion vectors.

2 Motion estimation with global minimization schemes

2.1 Iterative methods based on global error minimization

Most of the motion estimation schemes are based on the formulation of some kind of continuity constraint, such as the continuity of image intensity. A property of the continuity constraints is that they impose *local* requirements. A disadvantage of methods using local requirements is that they are extremely sensitive to noise. In this section we try to optimize the continuity constraints over the complete image. An extension to incorporate continuity with respect to the time coordinate is also given. The methods amount to the solution of a large system of linear equations. Iterative techniques are essential for the solution of the problem, because the required computer storage and computation time of direct matrix inversion methods are prohibitive. The solution of the system of equations will be obtained with the aid of a continuous version of the conjugate gradient technique. The latter technique converges to the global optimum for the pertaining quadratic error criterion.

For other error criteria, the conjugate gradient technique might be less suitable. However, the quadratic error criterion is a natural choice for most physical systems because it minimizes the energy difference between two quantities. If the data suffers from severe outliers, then the robustness might be increased with, for example, the mean-absolute-value error criterion. In this report only the widely used mean-squared error criterion is used because it leads to sufficiently accurate and stable results in nearly all cases of practical interest.

2.2 Vectorial displaced frame difference

The detection of motion can be based on Displaced Frame Difference (DFD) methods. Picture element (Pel)-recursive DFD schemes have been derived in the past. These schemes try to estimate the image motion on a pixel-by-pixel basis by minimizing a local error criterion, the Displaced Frame Difference [4]. A disadvantage is the poor convergence, if convergence is obtained at all. An additional disadvantage is the susceptibility to noise. In this section we try to arrive at a converging iterative scheme with improved stability where we minimize a vectorial version of the DFD-error in a least-mean square sense, i.e., globally, with a conjugate gradient technique. The only requirement is that the DFD can be linearized with respect to the pixel displacement.

2.2.1 Derivation

The starting point of our derivation is the formulation of continuity of intensity according to

$$I(\mathbf{x}, t) = I(\mathbf{x} + \mathbf{d}, t + \Delta t). \tag{2.1}$$

The deviation from this equation is expressed in the Displaced Frame Difference [4]:

$$\mathrm{dfd}(\mathbf{x}, \mathbf{d}) = I(\mathbf{x}, t) - I(\mathbf{x} + \mathbf{d}, t + \Delta t). \tag{2.2}$$

To arrive at the desired results we introduce a *vectorial* version $\mathbf{D}$ of the standard dfd according to

$$\mathbf{D} = (D_x, D_y), \tag{2.3}$$

with

$$\{D_x, D_y\} = \mathrm{dfd}(\mathbf{x}, \{\mathbf{d}_x, \mathbf{d}_y\}), \tag{2.4}$$

in which

$$\mathbf{d}_x = (d_x, 0) \tag{2.5}$$
$$\mathbf{d}_y = (0, d_y). \tag{2.6}$$

The value of the displacement $\mathbf{d}$ will be searched for in an iterative way [22]. The approximations of $\mathbf{d}$ at iteration n will be denoted by $\mathbf{d}^{(n)}$. A global error criterion at iteration n is introduced as

$$\mathrm{J}^{(n)} = \int_{\mathbf{x} \in \mathcal{S}} \|\mathbf{F}^{(n)}\|^2 d\mathbf{x}, \tag{2.7}$$

where $\mathbf{F}^{(n)} = \mathbf{D}(\mathbf{x}, \mathbf{d}^{(n)})$. If $J^{(n)} = 0$, we have $\mathbf{F}^{(n)} = \mathbf{0}, \forall \mathbf{x} \in \mathcal{S}$, and we have solved our problem, also in a local sense. We assume that $\mathbf{D}$ can be linearized, i.e.,

$$\mathbf{D}(\mathbf{x}, \alpha\mathbf{d}_1 + \beta\mathbf{d}_2) = \alpha\mathbf{D}(\mathbf{x}, \mathbf{d}_1) + \beta\mathbf{D}(\mathbf{x}, \mathbf{d}_2), \quad \forall \mathbf{d}_1, \mathbf{d}_2. \tag{2.8}$$

This assumption can be justified on grounds of proportionality of the dfd with respect to image shifts in a certain direction. The displacement field $\mathbf{d}^{(n)}$ is expanded in vectorial Fourier components $\boldsymbol{\phi}^{(n)} = \boldsymbol{\phi}^{(n)}(\mathbf{k})$ according to

$$\mathbf{d}^{(n)} = \int_{-\infty}^{\infty} \boldsymbol{\phi}^{(n)} e^{i\mathbf{k}\cdot\mathbf{x}} d\mathbf{k}, \tag{2.9}$$

with $\mathbf{k} = (k_x, k_y)$ the spatial frequencies in the (x, y)-directions. The constraint that $\mathbf{d}^{(n)}$ is real leads to symmetry properties in the spectral domain. In going from the $(n-1)$-st step to the n-th, we take

$$\boldsymbol{\phi}^{(n)} = \boldsymbol{\phi}^{(n-1)} + \eta^{(n)}\mathbf{g}^{(n)}, \tag{2.10}$$

in which $\mathbf{g}^{(n)}$ are the search directions and $\eta^{(n)}$ is a variational parameter to minimize $J^{(n)}$. We obtain

$$\mathbf{F}^{(n)} = \mathbf{F}^{(n-1)} - \eta^{(n)}\mathbf{f}^{(n)}, \tag{2.11}$$

with

$$\mathbf{f}^{(n)} = -\mathbf{D}\left(\mathbf{x}, \int_{-\infty}^{\infty} \mathbf{g}^{(n)} e^{i\mathbf{k}\cdot\mathbf{x}} d\mathbf{k}\right). \tag{2.12}$$

The error criterion can be written as

$$\begin{aligned} \mathrm{J}^{(n)} &= \int_{\mathbf{x}\in\mathcal{S}} \|\mathbf{F}^{(n-1)} - \eta^{(n)}\mathbf{f}^{(n)}\|^2 d\mathbf{x} && (2.13)\\ &= \mathrm{J}^{(n-1)} - 2\eta^{(n)}A^{(n)} + \left(\eta^{(n)}\right)^2 B^{(n)}, && (2.14) \end{aligned}$$

with

$$A^{(n)} = \int_{\mathbf{x}\in\mathcal{S}} \mathbf{F}^{(n-1)} \cdot \mathbf{f}^{(n)} d\mathbf{x}, \tag{2.15}$$

and

$$B^{(n)} = \int_{\mathbf{x}\in\mathcal{S}} \|\mathbf{f}^{(n)}\|^2 d\mathbf{x}. \tag{2.16}$$

The minimum of $\mathrm{J}^{(n)}$, as a function of $\eta^{(n)}$, is obtained at

$$\eta^{(n)} = \frac{A^{(n)}}{B^{(n)}}. \tag{2.17}$$

Using this particular value of $\eta^{(n)}$, we get

$$\mathrm{J}^{(n)} = \mathrm{J}^{(n-1)} - \frac{\left(A^{(n)}\right)^2}{B^{(n)}}, \tag{2.18}$$

and

$$\mathbf{F}^{(n)} = \mathbf{F}^{(n-1)} - \frac{A^{(n)}}{B^{(n)}}\mathbf{f}^{(n)}. \tag{2.19}$$

The latter expression leads to the orthogonality property

$$\int_{\mathbf{x}\in\mathcal{S}} \mathbf{F}^{(n)} \cdot \mathbf{f}^{(n)} d\mathbf{x} = 0, \tag{2.20}$$

which will be used later. Using the expression for $A^{(n)}$ and interchanging integrations, we can write

$$A^{(n)} = \int_{-\infty}^{\infty} \mathbf{s}^{(n-1)*} \cdot \mathbf{g}^{(n)} d\mathbf{k}, \tag{2.21}$$

in which

$$\mathbf{s}^{(n)} = -\left[\int_{\mathbf{x}\in\mathcal{S}} \mathbf{D}\left(\mathbf{x}, \mathbf{F}^{(n)}\right) e^{i\mathbf{k}\cdot\mathbf{x}} d\mathbf{x}\right]^{*}. \tag{2.22}$$

The orthogonality property for $\mathbf{F}^{(n)}$ and $\mathbf{f}^{(n)}$ leads to an orthogonality property in the spectral domain:

$$\int_{-\infty}^{\infty} \mathbf{s}^{(n)*} \cdot \mathbf{g}^{(n)} d\mathbf{k} = 0. \tag{2.23}$$

Up til now, the search directions $\mathbf{g}^{(n)}$ have been completely arbitrary. We take the conjugate gradient directions

$$\mathbf{g}^{(n)} = \mathbf{s}^{(n-1)} + \frac{A^{(n)}}{A^{(n-1)}} \mathbf{g}^{(n-1)}, n \geq 2, \tag{2.24}$$

while

$$\mathbf{g}^{(1)} = \mathbf{s}^{(0)}. \tag{2.25}$$

Substituting these expressions in Eq. (2.21) and using the orthogonality relation Eq. (2.20), we obtain

$$A^{(n)} = \int_{-\infty}^{\infty} \|\mathbf{s}^{(n-1)}\|^2 d\mathbf{k}. \tag{2.26}$$

A preconditioned version of the conjugate gradient scheme is obtained by introducing a preconditioner P and its adjoint P^* [23] according to

$$\mathbf{g}^{(n)} = P^* P \mathbf{s}^{(n-1)} + \frac{A^{(n)}}{A^{(n-1)}} \mathbf{g}^{(n-1)}, n \geq 2, \tag{2.27}$$

while

$$\mathbf{g}^{(1)} = P^* P \mathbf{s}^{(0)}. \tag{2.28}$$

The preconditioner is chosen in such a way that it approximates the inverse operator of the problem at hand. Substituting these expressions in Eq. (2.21) and using the orthogonality relation Eq. (2.20), we obtain

$$A^{(n)} = \int_{-\infty}^{\infty} \|P\mathbf{s}^{(n-1)}\|^2 d\mathbf{k}. \tag{2.29}$$

Useful results are often obtained by using the inverse of the least-squares diagonal [24].

2.2.2 Properties

A few observations can be made regarding the properties and the implementation of the iteration scheme.

- Provided the linearity assumption holds, the error $\mathrm{J}^{(n)}$ decreases at each iteration step provided $A^{(n)} > 0$. From Eq. (2.29) we can see that $A^{(n)}$ is real and positive, unless $\mathrm{s}^{(n-1)}$ vanishes. However, in the latter case we have arrived at the exact minimum in the iteration $n-1$.
- The evaluation of $\mathbf{D}$ for different displacements can be performed with interpolation of I, such as with bilinear interpolation.
- The major computational task at each iteration is concerned with the evaluation of four two-dimensional Fourier integrals which can be computed efficiently with forward and inverse FFTs.
- Memory requirements are modest: the iteration scheme is a full 2D least-squares minimization scheme without the memory requirements of standard matrix inversion methods.
- Motion compensation is possible by using the results for the $k_x = 0, k_y = 0$ component.
- The problem should be scaled properly because of the non-linear dependence of $\mathbf{D}$ on $\mathbf{x}$.

2.2.3 Iteration scheme

The complete iteration scheme can be found below. The iteration scheme will be started with zero estimates.

- Initialization

$$\mathbf{d}^{(0)} = \mathbf{0}$$
$$\mathbf{F}^{(0)} = \mathbf{D}(\mathbf{x}, \mathbf{0})$$
$$J^{(0)} = \int_{\mathbf{x}\in\mathcal{S}} \|\mathbf{F}^{(0)}\|^2 d\mathbf{x}$$
$$\boldsymbol{\phi}^{(0)} = \mathbf{0}$$
$$n = 0$$

- Start iteration

$$\mathbf{s}^{(n)} = -\int_{\mathbf{x}\in\mathcal{S}} \mathbf{D}\left(\mathbf{x}, \mathbf{F}^{(n)}\right) e^{-i\mathbf{k}\cdot\mathbf{x}} d\mathbf{x}$$
$$n = n + 1$$

$$A^{(n)} = \int_{-\infty}^{\infty} \|\mathbf{s}^{(n-1)}\|^2 d\mathbf{k}$$

$$\mathbf{g}^{(n)} = \begin{cases} \mathbf{s}^{(0)} & n = 1 \\ \mathbf{s}^{(n-1)} + \frac{A^{(n)}}{A^{(n-1)}} \mathbf{g}^{(n-1)} & n > 1 \end{cases}$$

$$\mathbf{f}^{(n)} = -\mathbf{D}\left(\mathbf{x}, \int_{-\infty}^{\infty} \mathbf{g}^{(n)} e^{i\mathbf{k}\cdot\mathbf{x}} d\mathbf{k}\right)$$

$$B^{(n)} = \int_{\mathbf{x}\in S} \|\mathbf{f}^{(n)}\|^2 d\mathbf{x}$$

$$\eta^{(n)} = \frac{A^{(n)}}{B^{(n)}}$$

$$\phi^{(n)} = \phi^{(n-1)} + \eta^{(n)} \mathbf{g}^{(n)}$$

$$\mathbf{F}^{(n)} = \mathbf{F}^{(n-1)} - \eta^{(n)} \mathbf{f}^{(n)}$$

$$\mathrm{J}^{(n)} = \mathrm{J}^{(n-1)} - \eta^{(n)} A^{(n)}$$

- End iteration

$$\mathbf{d}^{(n)} = \int_{-\infty}^{\infty} \phi^{(n)} e^{i\mathbf{k}\cdot\mathbf{x}} d\mathbf{k}$$

2.3 Gradient method with smoothness constraints

The detection of motion can also be based on spatial and temporal image gradients [11]. The equivalence of gradient methods and correlation based methods has been noted [25]. The gradient schemes try to estimate the pixel motion by minimizing a local error criterion based on the continuity of image intensity [11]. The velocity vector is obtained by a global minimization of the gradient equation with a conjugate gradient technique. Smoothness constraints are imposed which simultaneously minimize the variation in the estimated velocity in space and time. Additionally, simplified schemes are given which are based on the normal component of velocity.

2.3.1 Derivation

We start our derivation by recalling the so-called gradient equation, which can be obtained from linearization of Eq. (2.2) (see [11]):

$$\partial_t I(\mathbf{x}, t) + \mathbf{v}(\mathbf{x}, t) \cdot \nabla I(\mathbf{x}, t) = 0, \tag{2.30}$$

where we have used $\mathbf{v} = \mathbf{d}/\Delta t$, and ∂_t denotes differentiation with respect to time. Pixel-wise solution of this equation for $\mathbf{v}$ leads to serious problems: if the gradient approaches zero then the result becomes unbounded. To overcome the latter problems, we define a global error criterion which is minimized in a least-squares

sense by imposing smoothness constraints, as in the error criterion of [12]. In this case, however, we also impose a smoothness constraint in the time direction. The total error criterion becomes:

$$\mathrm{J} = \int_{t\in\mathcal{T}} dt \int_{\mathbf{x}\in\mathcal{S}} \Big\{ [\partial_t I + \mathbf{v}\cdot\nabla I]^2 + \alpha \left[\|\nabla v_x\|^2 + \|\nabla v_y\|^2 \right] + \beta \|\partial_t \mathbf{v}\|^2 \Big\}\, d\mathbf{x}, \quad (2.31)$$

The error criterion is minimized with a conjugate gradient technique. The global error criterion at iteration n is written as

$$\mathrm{J}^{(n)} = \int_{t\in\mathcal{T}} dt \int_{\mathbf{x}\in\mathcal{S}} \left(|F^{(n)}|^2 + \|\mathbf{F}_x^{(n)}\|^2 + \|\mathbf{F}_y^{(n)}\|^2 + \|\mathbf{F}_t^{(n)}\|^2 \right) d\mathbf{x}, \quad (2.32)$$

where

$$F^{(n)} = \partial_t I(\mathbf{x},t) + \mathbf{v}^{(n)}(\mathbf{x},t)\cdot\nabla I(\mathbf{x},t), \quad (2.33)$$

$$\mathbf{F}_{x,y}^{(n)} = \alpha^{1/2}\nabla v_{x,y}^{(n)} \quad (2.34)$$

$$\mathbf{F}_t^{(n)} = \beta^{1/2}\partial_t \mathbf{v}^{(n)} \quad (2.35)$$

and $\mathbf{v}^{(n)} = (v_x^{(n)}, v_y^{(n)})$ the approximation of $\mathbf{v}$ at iteration n. The velocity field $\mathbf{v}^{(n)}$ is expanded in vectorial Fourier components $\boldsymbol{\phi}^{(n)} = \boldsymbol{\phi}^{(n)}(\mathbf{k},\omega)$ according to

$$\mathbf{v}^{(n)} = \int_{-\infty}^{\infty} d\omega \int_{-\infty}^{\infty} \boldsymbol{\phi}^{(n)} e^{i(\mathbf{k}\cdot\mathbf{x}-\omega t)} d\mathbf{k}, \quad \mathbf{x}\in\mathcal{S}, t\in\mathcal{T}, \quad (2.36)$$

with $\mathbf{k} = (k_x, k_y)$ the spatial frequencies in the (x,y)-directions. The constraint that $\mathbf{v}^{(n)}$ is real leads to symmetry properties in the spectral domain. In going from the $(n-1)$-st step to the n-th, we take

$$\boldsymbol{\phi}^{(n)} = \boldsymbol{\phi}^{(n-1)} + \eta^{(n)}\mathbf{g}^{(n)}. \quad (2.37)$$

We obtain

$$\{F^{(n)}, \mathbf{F}_{x,y,t}^{(n)}\} = \{F^{(n-1)}, \mathbf{F}_{x,y,t}^{(n-1)}\} - \eta^{(n)}\{f^{(n)}, \mathbf{f}_{x,y,t}^{(n)}\}, \quad (2.38)$$

with

$$f^{(n)} = -\nabla I \cdot \int_{-\infty}^{\infty} d\omega \int_{-\infty}^{\infty} \mathbf{g}^{(n)} e^{i(\mathbf{k}\cdot\mathbf{x}-\omega t)} d\mathbf{k}, \quad (2.39)$$

$$\mathbf{f}_{x,y}^{(n)} = -i\alpha^{1/2} \int_{-\infty}^{\infty} d\omega \int_{-\infty}^{\infty} \mathbf{k} g_{x,y}^{(n)} e^{i(\mathbf{k}\cdot\mathbf{x}-\omega t)} d\mathbf{k}, \quad (2.40)$$

$$\mathbf{f}_t^{(n)} = i\beta^{1/2} \int_{-\infty}^{\infty} d\omega\, \omega \int_{-\infty}^{\infty} g_{x,y}^{(n)} e^{i(\mathbf{k}\cdot\mathbf{x}-\omega t)} d\mathbf{k}, \tag{2.41}$$

The error criterion can be written as

$$\mathrm{J}^{(n)} = \mathrm{J}^{(n-1)} - 2\eta^{(n)} A^{(n)} + \left(\eta^{(n)}\right)^2 B^{(n)}, \tag{2.42}$$

with

$$A^{(n)} = \int_{t\in\mathcal{T}} dt \int_{\mathbf{x}\in\mathcal{S}} \left(F^{(n-1)} f^{(n)} + \mathbf{F}_x^{(n-1)} \cdot \mathbf{f}_x^{(n)} + \mathbf{F}_y^{(n-1)} \cdot \mathbf{f}_y^{(n)} + \mathbf{F}_t^{(n-1)} \cdot \mathbf{f}_t^{(n)} \right) d\mathbf{x}, \tag{2.43}$$

and

$$B^{(n)} = \int_{t\in\mathcal{T}} dt \int_{\mathbf{x}\in\mathcal{S}} \left(|f^{(n)}|^2 + \|\mathbf{f}_x^{(n)}\|^2 + \|\mathbf{f}_y^{(n)}\|^2 + \|\mathbf{f}_t^{(n)}\|^2 \right) d\mathbf{x}. \tag{2.44}$$

The minimum of $\mathrm{J}^{(n)}$, as a function of $\eta^{(n)}$, is obtained at

$$\eta^{(n)} = \frac{A^{(n)}}{B^{(n)}}. \tag{2.45}$$

Using this particular value of $\eta^{(n)}$, we get

$$\mathrm{J}^{(n)} = \mathrm{J}^{(n-1)} - \frac{\left(A^{(n)}\right)^2}{B^{(n)}}, \tag{2.46}$$

and

$$\{F^{(n)}, \mathbf{F}_{x,y,t}^{(n)}\} = \{F^{(n-1)}, \mathbf{F}_{x,y,t}^{(n-1)}\} - \frac{A^{(n)}}{B^{(n)}} \{f^{(n)}, \mathbf{f}_{x,y,t}^{(n)}\}. \tag{2.47}$$

The latter expression leads to the orthogonality property

$$\int_{t\in\mathcal{T}} dt \int_{\mathbf{x}\in\mathcal{S}} \left(F^{(n)} f^{(n)} + \mathbf{F}_x^{(n)} \cdot \mathbf{f}_x^{(n)} + \mathbf{F}_y^{(n)} \cdot \mathbf{f}_y^{(n)} + \mathbf{F}_t^{(n)} \cdot \mathbf{f}_t^{(n)} \right) d\mathbf{x} = 0, \tag{2.48}$$

which will be used later. Using the expression for $A^{(n)}$ and interchanging integrations, we can write

$$A^{(n)} = \int_{-\infty}^{\infty} d\omega \int_{-\infty}^{\infty} \mathbf{s}^{(n-1)*} \cdot \mathbf{g}^{(n)} d\mathbf{k}, \tag{2.49}$$

in which

$$s_x^{(n)} = \left[\int_{t\in\mathcal{T}} dt \int_{\mathbf{x}\in\mathcal{S}} \left(-F^{(n)} \partial_x I - i\alpha^{1/2} \mathbf{k} \cdot \mathbf{F}_x^{(n)} + i\beta^{1/2} \omega F_{tx}^{(n)} \right) e^{i(\mathbf{k}\cdot\mathbf{x}-\omega t)} d\mathbf{x} \right]^*, \tag{2.50}$$

$$s_y^{(n)} = \left[\int_{t\in\mathcal{T}} dt \int_{\mathbf{x}\in\mathcal{S}} \left(-F^{(n)} \partial_y I - i\alpha^{1/2} \mathbf{k} \cdot \mathbf{F}_y^{(n)} + i\beta^{1/2} \omega F_{ty}^{(n)} \right) e^{i(\mathbf{k}\cdot\mathbf{x}-\omega t)} d\mathbf{x} \right]^*, \tag{2.51}$$

with $\mathbf{F}_t = (F_{tx}, F_{ty})$. The orthogonality property for $\{F^{(n)}, \mathbf{F}_{x,y,t}^{(n)}\}$ and $\{f^{(n)}, \mathbf{f}_{x,y,t}^{(n)}\}$ leads to an orthogonality property in the spectral domain:

$$\int_{-\infty}^{\infty} d\omega \int_{-\infty}^{\infty} \mathbf{s}^{(n)*} \cdot \mathbf{g}^{(n)} d\mathbf{k} = 0. \tag{2.52}$$

Up til now, the search directions $\mathbf{g}^{(n)}$ have been completely arbitrary. We take the conjugate gradient directions

$$\mathbf{g}^{(n)} = \mathbf{s}^{(n-1)} + \frac{A^{(n)}}{A^{(n-1)}} \mathbf{g}^{(n-1)}, n \geq 2, \tag{2.53}$$

while

$$\mathbf{g}^{(1)} = \mathbf{s}^{(0)}. \tag{2.54}$$

Substituting these expressions in Eq. (2.49) and using the orthogonality relation Eq. (2.48), we obtain

$$A^{(n)} = \int_{-\infty}^{\infty} d\omega \int_{-\infty}^{\infty} \|\mathbf{s}^{(n-1)}\|^2 d\mathbf{k}. \tag{2.55}$$

A preconditioned version of the conjugate gradient scheme is obtained by introducing a preconditioner P according to [23]

$$\mathbf{g}^{(n)} = P^* P \mathbf{s}^{(n-1)} + \frac{A^{(n)}}{A^{(n-1)}} \mathbf{g}^{(n-1)}, n \geq 2, \tag{2.56}$$

while

$$\mathbf{g}^{(1)} = P^* P \mathbf{s}^{(0)}, \tag{2.57}$$

where P^* is the adjoint of P. Substituting these expressions in Eq. (2.21) and using the orthogonality relation Eq. (2.20), we obtain

$$A^{(n)} = \int_{-\infty}^{\infty} d\omega \int_{-\infty}^{\infty} \|P\mathbf{s}^{(n-1)}\|^2 d\mathbf{k}. \tag{2.58}$$

Useful results are often obtained by simply using the inverse of the least-squares matrix diagonal [24], such as in

$$Ps_{x,y}^{(n)} = \left[\int_{t\in\mathcal{T}} dt \int_{\mathbf{x}\in\mathcal{S}} \left(|\partial_{x,y} I|^2 + \alpha \|\mathbf{k}\|^2 + \beta\omega^2 \right) d\mathbf{x} \right]^{-1/2} s_{x,y}^{(n)}, \tag{2.59}$$

2.3.2 Properties

- The error $J^{(n)}$ decreases at each iteration step provided $A^{(n)} > 0$. From Eq. (2.58) we can see that $A^{(n)}$ is real and positive, unless $s^{(n-1)}$ vanishes. However, in the latter case we have arrived at the exact minimum in the iteration $n-1$.
- The major computational task at each iteration is concerned with the evaluation of four two-dimensional Fourier integrals which can be computed efficiently with forward and inverse FFTs.
- Memory requirements are modest: the iteration scheme is a full 2D least-squares minimization scheme without the memory requirements of standard matrix inversion methods.
- Motion compensation is possible by using the results for the $k_x = 0, k_y = 0$ component.
- It should be noticed that $\mathbf{v}$ is a vector with two spatial components. Therefore, the total number of unknowns is twice the number of equations if standard FFTs are used for computing the spatial and spectral integrals. As a consequence, the number of spectral components should be limited to a maximum of half the number of $\mathbf{v}$-vectors.
- For subsequent frames, the iterative scheme can be started with the result $\mathbf{v}$ of the previous frame.

2.3.3 Iteration scheme

The starting value of the iteration scheme is not critical because the convergence is assured. For simplicity, the iteration scheme will be started with zero estimates.

- Initialization

$$\mathbf{v}^{(0)} = \mathbf{0}$$

$$F^{(0)} = \partial_t I$$

$$\mathbf{F}^{(0)}_{x,y,t} = \mathbf{0}$$

$$J^{(0)} = \int_{t\in\mathcal{T}} dt \int_{\mathbf{x}\in\mathcal{S}} |F^{(0)}|^2 d\mathbf{x}$$

$$\boldsymbol{\phi}^{(0)} = \mathbf{0}$$

$$n = 0$$

$$P_{x,y} = \left[\int_{t\in\mathcal{T}} dt \int_{\mathbf{x}\in\mathcal{S}} \left(|\partial_{x,y} I|^2 + \alpha\|\mathbf{k}\|^2 + \beta\omega^2\right) d\mathbf{x}\right]^{-1/2},$$

- Start iteration

$$s_x^{(n)} = \left[\int_{t\in\mathcal{T}} dt \int_{\mathbf{x}\in\mathcal{S}} \left(-F^{(n)}\partial_x I - i\alpha^{1/2}\mathbf{k}\cdot\mathbf{F}_x^{(n)} + i\beta^{1/2}\omega F_{tx}^{(n)} \right) e^{i(\mathbf{k}\cdot\mathbf{x}-\omega t)} d\mathbf{x} \right]^*$$

$$s_y^{(n)} = \left[\int_{t\in\mathcal{T}} dt \int_{\mathbf{x}\in\mathcal{S}} \left(-F^{(n)}\partial_y I - i\alpha^{1/2}\mathbf{k}\cdot\mathbf{F}_y^{(n)} + i\beta^{1/2}\omega F_{ty}^{(n)} \right) e^{i(\mathbf{k}\cdot\mathbf{x}-\omega t)} d\mathbf{x} \right]^*$$

$$n = n + 1$$

$$A^{(n)} = \int_{-\infty}^{\infty} d\omega \int_{-\infty}^{\infty} \|P\mathbf{s}^{(n-1)}\|^2 d\mathbf{k}$$

$$\mathbf{g}^{(n)} = \begin{cases} P^2\mathbf{s}^{(0)} & n = 1 \\ P^2\mathbf{s}^{(n-1)} + \frac{A^{(n)}}{A^{(n-1)}}\mathbf{g}^{(n-1)} & n > 1 \end{cases}$$

$$f^{(n)} = -\nabla I \cdot \int_{-\infty}^{\infty} d\omega \int_{-\infty}^{\infty} \mathbf{g}^{(n)} e^{i(\mathbf{k}\cdot\mathbf{x}-\omega t)} d\mathbf{k}$$

$$\mathbf{f}_{x,y}^{(n)} = -i\alpha^{1/2} \int_{-\infty}^{\infty} d\omega \int_{-\infty}^{\infty} \mathbf{k} g_{x,y}^{(n)} e^{i(\mathbf{k}\cdot\mathbf{x}-\omega t)} d\mathbf{k},$$

$$\mathbf{f}_t^{(n)} = i\beta^{1/2} \int_{-\infty}^{\infty} d\omega\, \omega \int_{-\infty}^{\infty} \mathbf{g}^{(n)} e^{i(\mathbf{k}\cdot\mathbf{x}-\omega t)} d\mathbf{k},$$

$$B^{(n)} = \int_{t\in\mathcal{T}} dt \int_{\mathbf{x}\in\mathcal{S}} \left(|f^{(n)}|^2 + \|\mathbf{f}_x^{(n)}\|^2 + \|\mathbf{f}_y^{(n)}\|^2 + \|\mathbf{f}_t^{(n)}\|^2 \right) d\mathbf{x}$$

$$\eta^{(n)} = \frac{A^{(n)}}{B^{(n)}}$$

$$\boldsymbol{\phi}^{(n)} = \boldsymbol{\phi}^{(n-1)} + \eta^{(n)}\mathbf{g}^{(n)}$$

$$F^{(n)} = F^{(n-1)} - \eta^{(n)} f^{(n)}$$

$$\mathbf{F}_{x,y,t}^{(n)} = \mathbf{F}_{x,y,t}^{(n-1)} - \eta^{(n)}\mathbf{f}_{x,y,t}^{(n)}$$

$$\mathrm{J}^{(n)} = \mathrm{J}^{(n-1)} - \eta^{(n)} A^{(n)}$$

- End iteration

$$\mathbf{v}^{(n)} = \int_{-\infty}^{\infty} d\omega \int_{-\infty}^{\infty} \boldsymbol{\phi}^{(n)} e^{i(\mathbf{k}\cdot\mathbf{x}-\omega t)} d\mathbf{k}$$

2.3.4 Results

In this section we show an example of the algorithm of subsection 2.3.3 for two images. Consequently, we set $\beta = 0$. The velocity estimates are obtained after low-pass filtering of the images. It can be seen in Figs. 2.2 and 2.3 that the estimated velocity of the middle part of the car is different from the estimated velocity near the boundaries. Only the object boundaries normal to movement are detected. This is a well-known problem [11] which can be attacked by incorporating other methods, such as contour detection. For some applications, such as motion detection, it is not very important to know the motion vectors that are parallel to the object boundaries.

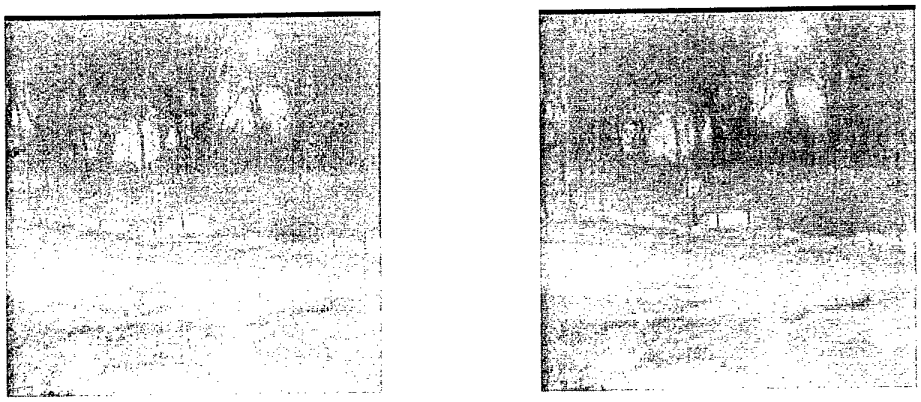

Figure 2.1: Two consecutive image frames.

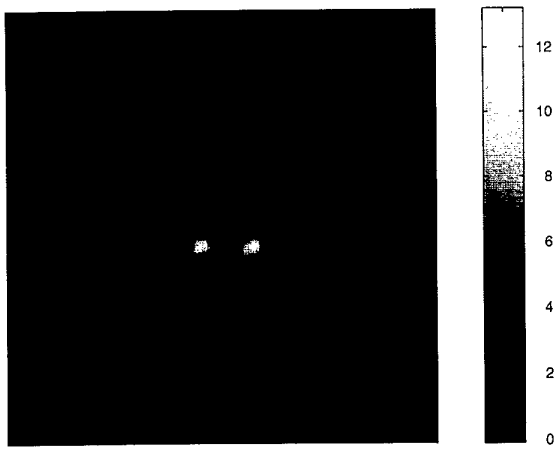

Figure 2.2: Computed velocity of Fig. 2.1.

Figure 2.3: Image of Fig. 2.1 with indicated velocity vectors.

Figure 2.4: Image of Fig. 2.1 with superimposed and thresholded velocity.

2.4 Scalar velocity method

It is possible to reduce the number of unknowns by reducing the vectorial velocity to the scalar velocity component in the direction of the spatial gradient (see also: [11]). Without using the smoothness constraints, the continuity requirement of the previous section can be written as

$$\partial_t I(\mathbf{x},t) + \|\mathbf{v}(\mathbf{x})\| \, \|\nabla I(\mathbf{x},t)\| \cos\theta(\mathbf{x}) = 0, \tag{2.60}$$

with $\theta = \angle(\mathbf{v}, \nabla I)$ the angle between the gradient and the velocity vector. If we write

$$v(\mathbf{x}) = \|\mathbf{v}(\mathbf{x})\| \cos\theta(\mathbf{x}), \tag{2.61}$$

we obtain

$$\partial_t I(\mathbf{x},t) + v(\mathbf{x}) \|\nabla I(\mathbf{x},t)\| = 0. \tag{2.62}$$

Instead of solving for the two vectorial components of $\mathbf{v}$ we now try to solve for the scalar component v. The iteration scheme will be given without derivation.

2.4.1 Iteration scheme

- Initialization

$$v^{(0)} = 0$$

$$F^{(0)} = \partial_t I$$

$$J^{(0)} = \int_{\mathbf{x}\in\mathcal{S}} |F^{(0)}|^2 d\mathbf{x}$$

$$\phi^{(0)} = 0$$

$$n = 0$$

- Start iteration

$$s^{(n)} = -\int_{\mathbf{x}\in\mathcal{S}} F^{(n)} \|\nabla I\| e^{-i\mathbf{k}\cdot\mathbf{x}} d\mathbf{x}$$

$$n = n + 1$$

$$A^{(n)} = \int_{-\infty}^{\infty} |s^{(n-1)}|^2 d\mathbf{k}$$

$$g^{(n)} = \begin{cases} s^{(0)} & n = 1 \\ s^{(n-1)} + \frac{A^{(n)}}{A^{(n-1)}} g^{(n-1)} & n > 1 \end{cases}$$

$$f^{(n)} = -\|\nabla I\| \int_{-\infty}^{\infty} g^{(n)} e^{i\mathbf{k}\cdot\mathbf{x}} d\mathbf{k}$$

$$B^{(n)} = \int_{\mathbf{x}\in\mathcal{S}} |f^{(n)}|^2 d\mathbf{x}$$

$$\eta^{(n)} = \frac{A^{(n)}}{B^{(n)}}$$

$$\phi^{(n)} = \phi^{(n-1)} + \eta^{(n)} g^{(n)}$$

$$F^{(n)} = F^{(n-1)} - \eta^{(n)} f^{(n)}$$

$$\mathrm{J}^{(n)} = \mathrm{J}^{(n-1)} - \eta^{(n)} A^{(n)}$$

- End iteration

$$v^{(n)} = \int_{-\infty}^{\infty} \phi^{(n)} e^{i\mathbf{k}\cdot\mathbf{x}} d\mathbf{k}$$

2.4.2 Example

The gradient method based on the scalar velocity was applied to recorded image frames. Two consecutive frames can be found in Fig. 2.5. In Fig. 2.6, the computed velocity is shown. Figure 2.7 shows the first image frame in which a detection limit has been used to indicate image motion. The images have a size of 256 × 256 pixels. About six iterations were used. This is not critical, however: often only one iteration leads to sufficient convergence.

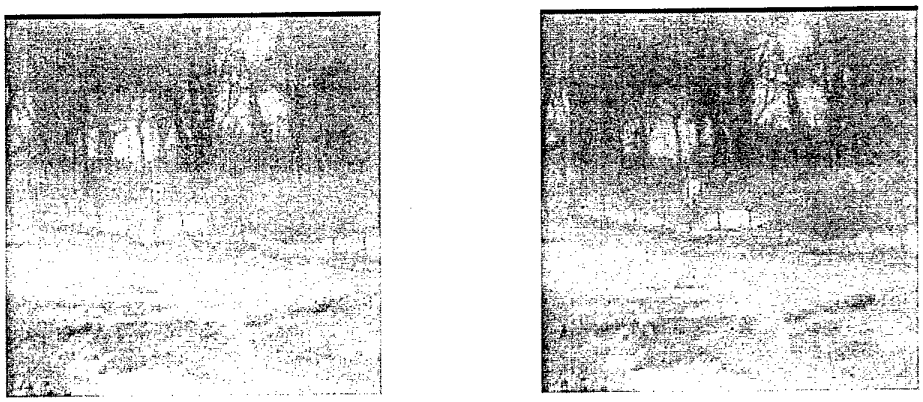

Figure 2.5: Two consecutive image frames.

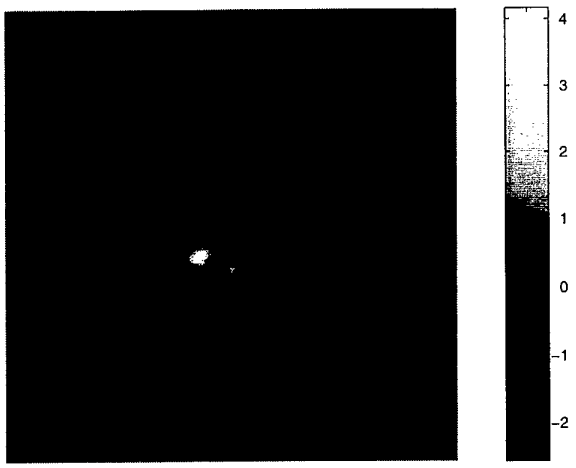

Figure 2.6: Normal velocity computed from the two consecutive image frames.

Figure 2.7: First image frame with indicated image velocity.

2.5 Scalar velocity method with smoothness constraint in time

As a last example, a scheme is given which uses scalar velocity, Fourier descriptions in time only, and a smoothness constraint in time. Then, the error criterion becomes

$$\mathrm{J} = \int_{t\in\mathcal{T}} dt \int_{\mathbf{x}\in\mathcal{S}} \left\{ [\partial_t I + v\|\nabla I\|]^2 + \beta|\partial_t v|^2 \right\} d\mathbf{x}. \tag{2.63}$$

The iteration scheme will be given without derivation. An advantage of this scheme is the relatively low computational complexity, because the temporal Fourier transforms are one-dimensional and relatively short. For very short FFT's, the pertinent matrix may consist of only ones and zeros, which makes the scheme interesting for hardware implementations.

2.5.1 Iteration scheme

- Initialization

$$v^{(0)} = 0$$
$$F^{(0)} = \partial_t I$$
$$F_t^{(0)} = 0$$
$$J^{(0)} = \int_{\mathbf{x}\in\mathcal{S}} |F^{(0)}|^2 d\mathbf{x}$$
$$\phi^{(0)} = 0$$

$$n = 0$$

- Start iteration

$$s^{(n)} = -\left[\int_{\mathbf{x}\in\mathcal{S}} d\mathbf{x} \int_{t\in\mathcal{T}} \left(F^{(n)}\|\nabla I\| + i\beta^{1/2}\omega\right) e^{-i\omega t} dt\right]^*$$

$$n = n + 1$$

$$A^{(n)} = \int_{-\infty}^{\infty} |s^{(n-1)}|^2 d\omega$$

$$g^{(n)} = \begin{cases} s^{(0)} & n = 1 \\ s^{(n-1)} + \frac{A^{(n)}}{A^{(n-1)}} g^{(n-1)} & n > 1 \end{cases}$$

$$f^{(n)} = -\|\nabla I\| \int_{-\infty}^{\infty} g^{(n)} e^{-i\omega t} d\omega$$

$$f_t^{(n)} = -i\beta^{1/2} \int_{-\infty}^{\infty} \omega g^{(n)} e^{-i\omega t} d\omega$$

$$B^{(n)} = \int_{t\in\mathcal{T}} dt \int_{\mathbf{x}\in\mathcal{S}} \left(|f^{(n)}|^2 + |f_t^{(n)}|^2\right) d\mathbf{x}$$

$$\eta^{(n)} = \frac{A^{(n)}}{B^{(n)}}$$

$$\phi^{(n)} = \phi^{(n-1)} + \eta^{(n)} g^{(n)}$$

$$F^{(n)} = F^{(n-1)} - \eta^{(n)} f^{(n)}$$

$$F_t^{(n)} = F_t^{(n-1)} - \eta^{(n)} f_t^{(n)}$$

$$\mathrm{J}^{(n)} = \mathrm{J}^{(n-1)} - \eta^{(n)} A^{(n)}$$

- End iteration

$$v^{(n)} = \int_{-\infty}^{\infty} \phi^{(n)} e^{-i\omega t} d\omega$$

2.5.2 Multi-resolution analysis

The continuity equations of the preceding section are based on linearization of the displaced frame difference. Therefore, large-scale movements can only be determined from low-pass filtered images. In the present section, we define a multi-resolution scheme where image motion is determined from subsequent application of one of the gradient-based conjugate gradient schemes to low-pass filtered images. Each subsequent conjugate gradient calculation is performed with increasing cut-off frequency f_c, i.e., on a finer scale. After application of the conjugate gradient scheme, we fall back on the displaced frame difference by performing interpolation in the original image. The interpolated image, which is based on the velocity vector defined in the previous step, is used as a basis for

determining image motion on a finer scale. The basic idea is that we try to estimate the motion vector needed to get from the first image to the second image. The estimated second image is denoted by using a tilde above the different symbols. The procedure can be summarized in the following scheme (the symbol $**$ denotes a two-dimensional convolution):

- initialization

$$n = 0$$
$$\mathbf{d}^{(0)} = \mathbf{0}$$
$$\widetilde{I}^{(0)}(\mathbf{x}, t + \Delta t) = I(\mathbf{x}, t)$$
$$f_c^{(0)} = f_{c,\min}$$

- start iteration

$$I_F^{(n)}(\mathbf{x}, t + \Delta t) = \mathrm{LPF}(f_c^{(n)}) ** I(\mathbf{x}, t + \Delta t)$$
$$\widetilde{I}_F^{(n)}(\mathbf{x}, t + \Delta t) = \mathrm{LPF}(f_c^{(n)}) ** \widetilde{I}^{(n)}(\mathbf{x}, t + \Delta t)$$
$$n = n + 1$$
$$\text{solve } \mathbf{v}_F^{(n)} \text{ from } I_F^{(n-1)} - \widetilde{I}_F^{(n-1)} + \mathbf{v}_F^{(n)} \cdot \nabla I_F^{(n-1)} = 0$$
$$\mathbf{d}^{(n)} = \mathbf{d}^{(n-1)} + \Delta t\, \mathbf{v}_F^{(n)}$$
$$\widetilde{I}^{(n)}(\mathbf{x}, t + \Delta t) = I(\mathbf{x} - \mathbf{d}^{(n)}, t)$$
$$f_c^{(n)} = 2 f_c^{(n-1)}$$

- end iteration

$$\mathbf{v}^{(n)} = \frac{\mathbf{d}^{(n)}}{\Delta t}$$

2.6 Overall conclusion

Iterative techniques were applied to the estimation of motion in images. One method is based on a direct formulation using the displaced frame difference. A method which overcomes the scaling problems of the latter method is based on the linearization of the displaced frame difference, using additional smoothness constraints imposed on the vectorial velocity. An efficiency improvement results from the definition of the normal image velocity, thereby reducing the number of unknowns with a factor two. A continuous velocity field is an inherent property of the techniques. Subpixel displacements can be obtained with all three methods and multiresolution schemes are also discussed.

The computation of gradients, the setting of different filter characteristics and the optional use of weighting functions require further study. Furthermore, special precautions have to be taken to avoid folding contributions due to the periodicity associated with the Fourier or cosine/sine transforms.

3 References

[1] J.A. Leese, C.S. Novak, and V.R. Taylor. The determination of cloud pattern motions from geosynchronous satellite image data. *Pattern Recognition*, 2:279–292, 1970.

[2] J.A. Leese and C.S. Novak. An automated technique for obtaining cloud motion from geosynchronous satellite data using cross correlation. *Journal of Applied Meteorology*, 10:118–132, 1971.

[3] J.R. Jain and A.K. Jain. Displacement measurement and its application in interframe image coding. *IEEE Transactions on Communications*, COM-29:1799–1808, 1981.

[4] A.N. Netravali and J.D. Robbins. Motion-compensated television coding: part1. *The Bell System Technical Journal*, 58:631–670, 1979.

[5] D.R. Walker and K.R. Rao. Improved pel-recursive motion compensation. *IEEE Transactions on Communications*, COM-32:1128–1134, 1984.

[6] D.J. Le Gall. The mpeg video compression algorithm. *Image Communication*, 4:129–140, 1992.

[7] ISO/IEC. Information technology - coding of moving pictures and associated audio for digital storage media at up to about 1.5 mbit/s - part 2: video (iso 11172-2). Technical report, ISO/IEC, Geneve, 1993.

[8] G. Gupta and C. Chakrabarti. Architectures for hierarchical and other block matching algorithms. *IEEE Transactions on Circuits and Systems for Video Technology*, 5:477–489, 1995.

[9] B.F. Buxton and H. Buxton. Computation of optic flow from the motion of edge features in image sequences. *Image and Vision Computing*, 2:59–75, 1984.

[10] R. Kories and G. Zimmermann. Motion detection in image sequences: an evaluation of feature detectors. In *International Conference on Pattern Recognition 1984*, pages 778–780. IEEE, 1984.

[11] A. Singh. *Optic flow computation: a unified perspective.* IEEE Computer Society Press, Los Alamitos, 1991.

[12] B.K.P. Horn and B.G. Schunck. Determining optical flow. *Artificial Intelligence*, 17:185–203, 1981.

[13] H.-H. Nagel. Displacement vectors derived from second-order intensity variations in image sequences. *Computer Vision, Graphics, and Image Processing*, 21:85–117, 1983.

[14] A.M. Waxman, J. Wu, and F. Bergholm. Convected activation profiles and the measurement of visual motion. In *Proc. IEEE Computer Vision and Pattern Recognition*, pages 717–723. IEEE, 1988.

[15] D.J. Heeger. Optical flow from spatiotemporal filters. In *Proc. IEEE Computer Vision*, pages 181–190. IEEE, 1987.

[16] D.J. Fleet and A.D. Jepson. Computation of normal velocity from local phase information. In *Proc. IEEE Computer Vision and Pattern Recognition*, pages 379–386. IEEE, 1989.

[17] D.J. Fleet, A.D. Jepson, and M.R.M. Jenkin. Phase-based disparity measurement. *CVGIP: Image Understanding*, 53:199–210, 1991.

[18] W.J.C. Beck. Feasibility hardware bewegingsschatter. Technical Report FEL-93-A262, TNO-FEL, The Hague, 1994.

[19] Q.X. Wu. A correlation-relaxation-labeling framework for computing optical flow - template matching from a new perspective. *IEEE Transactions on Pattern Analysis and Machine Intelligence*, 17:843–853, 1995.

[20] P. Salembier, L. Toores, F. Meyer, and C. Gu. Region-based video coding using mathematical morphology. *Proceedings of the IEEE*, 83:843–857, 1995.

[21] A. Mitiche and P. Bouthemy. Computation and analysis of image motion: a synopsis of current problems and methods. *International Journal of Computer Vision*, 19:29–55, 1996.

[22] A.P. Berkhoff, P.M. van den Berg, and J.M. Thijssen. Iterative calculation of reflected and transmitted acoustic waves at a rough interface. *IEEE Trans Ultrason Ferroel Freq Contr*, 42:663–671, 1995.

[23] A.P. Berkhoff, J.M. Thijssen, and P.M. van den Berg. Ultrasound wave propagation through rough interfaces: iterative methods. *J Acoust Soc Am*, 99:1306–1314, 1996.

[24] G.H. Golub and C.F. van Loan. *Matrix Computations, 2nd ed.* The John Hopkins University Press, 1989.

[25] C.-M. Wu and D.-K. Yeh. A vlsi motion estimator for video image compression. *IEEE Transactions on Consumer Electronics*, 39:837–846, 1993.

4 Signature

[1] The author is indebted to Rob Lerou for the careful examination of the manuscript.

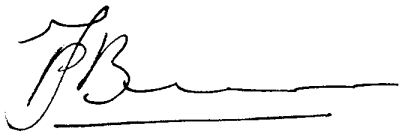

J.P. van Bezouwen
Group leader

A.P. Berkhoff
Author/Projectleader

[1]This report was typeset with LaTeX 2_ε using the APBreport document class.

REPORT DOCUMENTATION PAGE
(MOD-NL)

1. DEFENCE REPORT NO (MOD-NL)	2. RECIPIENT'S ACCESSION NO	3. PERFORMING ORGANIZATION REPORT NO
TD97-0074		FEL-96-B265
4. PROJECT/TASK/WORK UNIT NO	**5. CONTRACT NO**	**6. REPORT DATE**
25465	-	February 1997
7. NUMBER OF PAGES	**8. NUMBER OF REFERENCES**	**9. TYPE OF REPORT AND DATES COVERED**
27 (excl RDP & distribution list)	25	

10. TITLE AND SUBTITLE

Conjugate gradient schemes for motion estimation in image sequences

11. AUTHOR(S)

A.P. Berkhoff

12. PERFORMING ORGANIZATION NAME(S) AND ADDRESS(ES)

TNO Physics and Electronics Laboratory, PO Box 96864, 2509 JG The Hague, The Netherlands
Oude Waalsdorperweg 63, The Hague, The Netherlands

13. SPONSORING AGENCY NAME(S) AND ADDRESS(ES)

TNO Physics and Electronics Laboratory, PO Box 96864, 2509 JG The Hague, The Netherlands
Oude Waalsdorperweg 63, The Hague, The Netherlands

14. SUPPLEMENTARY NOTES

The classification designation Ongerubriceerd is equivalent to Unclassified, Stg. Confidentieel is equivalent to Confidential and Stg. Geheim is equivalent to Secret.

15. ABSTRACT (MAXIMUM 200 WORDS (1044 BYTE))

This report describes methods for the estimation of local motion in a sequence of images. The methods are based on a global minimization of a relevant error criterion using a conjugate gradient technique. The expansion of the displacement field is carried out with the use of basis functions according to a Fourier transform or a cosine/sine transform in space and time. These representations automatically result in a continuous displacement field where subpixel displacements can be detected. The error criterion can be based on a displacement vector for each pixel, but also on linearized versions in vectorial and scalar form, depending on the desired trade-off between computation time and accuracy.

16. DESCRIPTORS	IDENTIFIERS
Image processing Signal processing Digital techniques	Motion estimation Digital signal processing

17a.SECURITY CLASSIFICATION (OF REPORT)	17b.SECURITY CLASSIFICATION (OF PAGE)	17c.SECURITY CLASSIFICATION (OF ABSTRACT)
Ongerubriceerd	Ongerubriceerd	Ongerubriceerd

18. DISTRIBUTION AVAILABILITY STATEMENT	17d.SECURITY CLASSIFICATION (OF TITLES)
Unlimited Distribution	Ongerubriceerd

Distributielijst

1. Bureau TNO Defensieonderzoek
2. Directeur Wetenschappelijk Onderzoek en Ontwikkeling*)
3. HWO-KL
4. HWO-KLu*)
5. HWO-KM*)
6. HWO-CO*)

7 t/m 9. KMA, Bibliotheek

10. Directie TNO-FEL, t.a.v. Dr. J.W. Maas
11. Directie TNO-FEL, t.a.v. Ir. J.A. Vogel, daarna reserve
12. Archief TNO-FEL, in bruikleen aan M&P*)
13. Archief TNO-FEL, in bruikleen aan Ir. J.P. van Bezouwen
14. Archief TNO-FEL, in bruikleen aan Ir. A.W.P. van Heijningen
15. Archief TNO-FEL, in bruikleen aan Ir. A.C. van Koersel
16. Archief TNO-FEL, in bruikleen aan Ir. H.A.J.M. van Hoof
17. Archief TNO-FEL, in bruikleen aan Ir. P.C.R. Beukelman
18. Archief TNO-FEL, in bruikleen aan Ing. J.C.P. Bol
19. Archief TNO-FEL, in bruikleen aan Drs. R.J.L. Lerou
20. Archief TNO-FEL, in bruikleen aan Drs. K.W. Benoist
21. Archief TNO-FEL, in bruikleen aan Dr. ir. A.P. Berkhoff
22. Documentatie TNO-FEL
23. Reserve

TNO-PML, Bibliotheek**)
TNO-TM, Bibliotheek**)
TNO-FEL, Bibliotheek**)

Indien binnen de krijgsmacht extra exemplaren van dit rapport worden gewenst door personen of instanties die niet op de verzendlijst voorkomen, dan dienen deze aangevraagd te worden bij het betreffende Hoofd Wetenschappelijk Onderzoek of, indien het een K-opdracht betreft, bij de Directeur Wetenschappelijk Onderzoek en Ontwikkeling.

*) Beperkt rapport (titelblad, managementuittreksel, RDP en distributielijst).
**) RDP.